Bulletin of the Mineral Research and Exploration

http://bulletin.mta.gov.tr

The Uzunpınar (Boztepe-Kırşehir) Zn-Pb±Cu mineralization: A metamorphosed SEDEX-type mineralization in the Kırşehir Massif

Emre YILDIZ*[a], Ebru COŞKUN KAVUKÇU[b] and Yurdal GENÇ[c]

[a]*Hacettepe University, Faculty of Engineering, Department of Geological Engineering, Ankara, Türkiye*
[b]*General Directorate of Mineral Research and Exploration (MTA), Department of Mineral Analysis and Technology, Coordination of Mineralogy and Petrography Research, Ankara, Türkiye*
[c]*Hacettepe University, Faculty of Engineering, Department of Geological Engineering, Ankara, Türkiye*

Research Article

Keywords:
Zinc-Lead Mineralization, Kırşehir Massif, Metamorphic-Hosted Zn-Pb Mineralization.

ABSTRACT

The Uzunpınar (Boztepe-Kırşehir) Zn-Pb±Cu mineralization is hosted within the gneiss and marbles of Paleozoic Kalkanlıdağ Formation of the Central Anatolian Crystalline Complex. The rocks observed in the mineralization area are mica gneiss, marble, migmatite, and microgranite, which were formed through high-grade metamorphism and anatexis of pelitic and carbonate protoliths. The mineralization has a stratiform geometry which extends approximately 1,850 m in a NE-SW direction. Six distinct mineralization levels (horizons), exhibiting similar characteristics and thicknesses ranging from 3.1–32.10 m, have been identified hosted within gneisses and marbles. These levels comprise ore bands and disseminations with thicknesses of 0.1–8 cm, aligned parallel to the foliation. Ore minerals are sphalerite, galena, chalcopyrite, and minor scheelite, while gangue minerals are pyrite, marcasite, pyrrhotite, gahnite, and Ba-feldspar. In the Uzunpınar mineralization, the alignment of ore bands with the host rock foliation, the presence of coarse-grained euhedral opaque minerals, foam textures, gahnite, Ba-feldspar, and the high Fe content in sphalerites serve as evidence for the influence of metamorphism on the mineralization. The stratiform geometry, syngenetic origin, and metal and mineral paragenesis suggest a SEDEX origin for the mineralization, later metamorphosed together with its host rocks.

Received Date: 01.05.2025
Accepted Date: 31.10.2025

1. Introduction

The Central Anatolian Crystalline Complex (CACC) is one of the major metallogenic provinces of Türkiye, with its metamorphic rocks hosting a variety of sulfide and iron deposits. East of the study area, exhalative deposits formed prior to metamorphism are prominently hosted within metamorphic rocks. The Başçatak Pb-Zn-Cu sulfide mineralization (Yozgat-Akdağmadeni), Yenipazar polymetallic mineralization (Yozgat-Boğazlıyan), and Sarıkaya Fe-Mn mineralizations (Yozgat-Sarıkaya) are hosted within the metamorphic units of the CACC and are classified as representative examples of sedimentary origin (Bakanyıldız, 1973; Genç, 1998; Jacobs Minerals, 2013). Pre-metamorphic formation, syngenetic origin, pronounced effects of metamorphism on ore texture and mineralogical

Citation Info: Yıldız, E., Kavukçu, E. C., Genç, Y. 2025. The Uzunpınar (Boztepe-Kırşehir) Zn-Pb±Cu mineralization: A metamorphosed SEDEX-type mineralization in the Kırşehir Massif. Bulletin of the Mineral Research and Exploration 178, 95-112. https://doi.org/10.19111/bulletinofmre.1816238

**Corresponding author: Emre YILDIZ, yildizee@gmail.com*

composition, host rocks with similar lithological features, and stratiform morphologies can be listed as common features of these mineralizations. The protoliths of the mineralizations likely formed within the same sedimentary basin under similar and closely related depositional conditions (Çağatay and Arda, 1976; Genç, 1998, 2001; Çolakoğlu and Genç, 2001; Coşkun, 2009). Genç (1998, 2001) emphasized that the Akdağmadeni-Başçatak Pb-Zn-Cu mineralization represents a pre-metamorphic exhalative-sedimentary deposit, highlighting the geological and metallogenic significance of exhalative systems in the region. This interpretation has been corroborated by subsequent studies on the same mineralization by Çolakoğlu and Genç (2001), Coşkun (2009) and Gökce et al. (2024).

This study aims to determine the geological characteristics of the Uzunpınar (Boztepe–Kırşehir) Zn–Pb±Cu mineralization and to evaluate the effects of metamorphism on the mineralization. To achieve this, fieldwork, sampling, and laboratory analyses were conducted, including microscopic and microchemical studies to examine the characteristics of the mineralization.

The Uzunpınar mineralization is located 3 km northeast of Uzunpınar Village in Boztepe District, Kırşehir Province, and approximately 37 km northeast of Kırşehir city center. The study area encompassing the mineralization spans 9 km² (Figure 1).

2. Material and Method

Mapping and sampling activities have been carried out in the mineralization area. In particular, outcrops and mineralized floats have been mapped. During fieldwork, drill cores were logged, and 16 polished thin sections were prepared from these core samples. The thin and polished sections were prepared at the General Directorate of Mineral Research and Exploration (MTA) laboratories and analyzed using a Leica DM2500P modular polarizing microscope at Mineral Deposits and Ore Microscopy Laboratory of Hacettepe University. Scanning electron microscopy (SEM) imaging and microchemical SEM-EDS analyses were conducted using an FEI Inspect F50 SEM at MTA. To determine metal content, ore samples were collected from split drill cores. The samples were dried at 80 °C, crushed, and subsequently ground to a particle size of <75 µm. The powdered samples were digested using HF:HNO_3:$HClO_4$:HCl and analyzed for 48 elements via inductively coupled plasma-optical emission spectrometry (ICP-OES). For elements exceeding the upper detection limits of ICP-OES, atomic absorption spectrometry (AAS) was employed. Gold analysis involved cupellation of 50 g aliquots from the pulverized samples, followed by ICP-OES determination.

3. Geology

3.1. Regional Geology

The Uzunpınar Mineralization is situated within the geological domain of the Central Anatolian Massif (CAM) (Ketin, 1955), also referred to as the Central Anatolian Crystalline Complex (CACC; Göncüoğlu et al., 1991). The complex is divided into the northern Kırşehir and Akdağ sub-massifs and the southern Niğde sub-massif. The CACC metamorphics

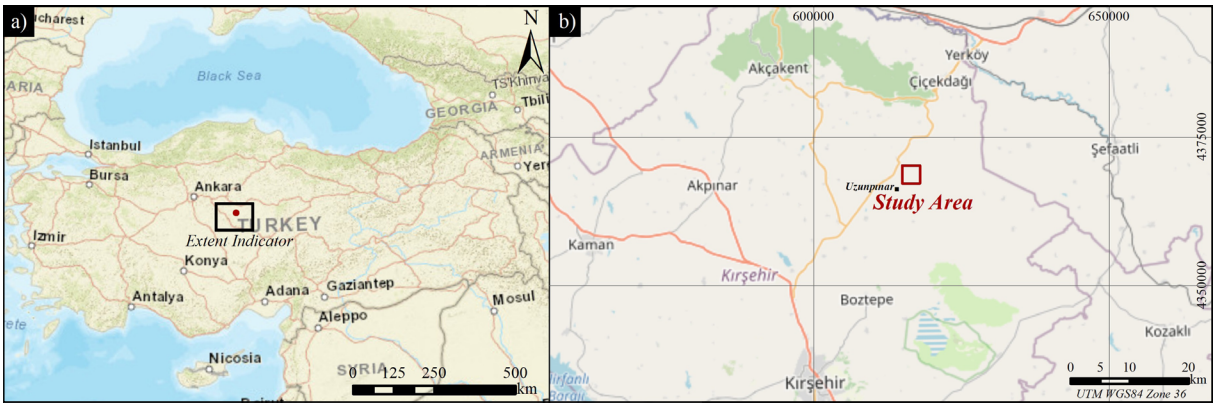

Figure 1- Site Location Map of the Study Area. Basemaps used, a) World Street Map (Esri, 2017), b) OpenStreetMap (OSM, 2024).

were metamorphosed under medium pressure-high temperature metamorphism conditions (Erkan, 1981).

The Uzunpınar mineralization is hosted by gneisses and marbles, metamorphic rocks of the Kırşehir Massif (Figure 2). Metamorphic conditions in the Kırşehir Massif range from greenschist to granulite facies, reflecting high-temperature and medium- to low-pressure regimes (Seymen, 1981). Pelitic schists and gneisses formed under upper amphibolite-facies conditions contain garnet, sillimanite, biotite, quartz, plagioclase, K-feldspar, ilmenite, cordierite, and spinel (hercynite). Thermobarometric results indicate that metapelitic rocks in the highest-grade regions of the Kırşehir Massif were buried to depths of 20–23 km (6–7 kbar) during thrusting, folding, and intrusion, with peak temperatures reaching 700–750°C in the most thermally elevated areas (e.g., near Kaman District) (Whitney et al., 2001). Erkan (1978) documented a north-northeastward increase in metamorphic grade, with the sillimanite-orthoclase zone—characterized by the presence of sillimanite—representing the highest metamorphic grade. The study area lies east of this sillimanite-orthoclase zone, and the diagnostic minerals sillimanite and garnet are widely observed in the vicinity of the Uzunpınar mineralization.

3.2. Geology of Uzunpınar Mineralization

In the region cover the study area, the Kırşehir Massif comprises from bottom to top the Bozçaldağ Formation, Kalkanlıdağ Formation, Kargasekmezdağ Quartzite Member, and Kervansaray Formation. These Paleozoic-aged formations are overlain by sedimentary and volcanic units of Eocene, Oligocene, Miocene, and Pliocene age (Figure 3).

The study area is predominantly underlain by the Kalkanlıdağ Formation, which comprises leucocratic, mesocratic, and melanocratic gneisses, biotite schists, pyroxene schists, and locally intercalated calc-schists containing wollastonite and diopside, with thin marble bands. The formation is interpreted to have been deposited in a marine environment dominated by mud sedimentation with occasional sandy intervals (Seymen, 1981, 1984). Transitional zones to the Tamadağ Formation include calc-silicate schists, meta-quartzites, and quartz schists (Seymen, 1981). These units are high-grade metamorphic rocks derived from pelitic and carbonate sedimentary protoliths, modified by regional metamorphism and anatexis.

Three main lithological units—mica gneiss, marble, and migmatite—are observed in intercalated

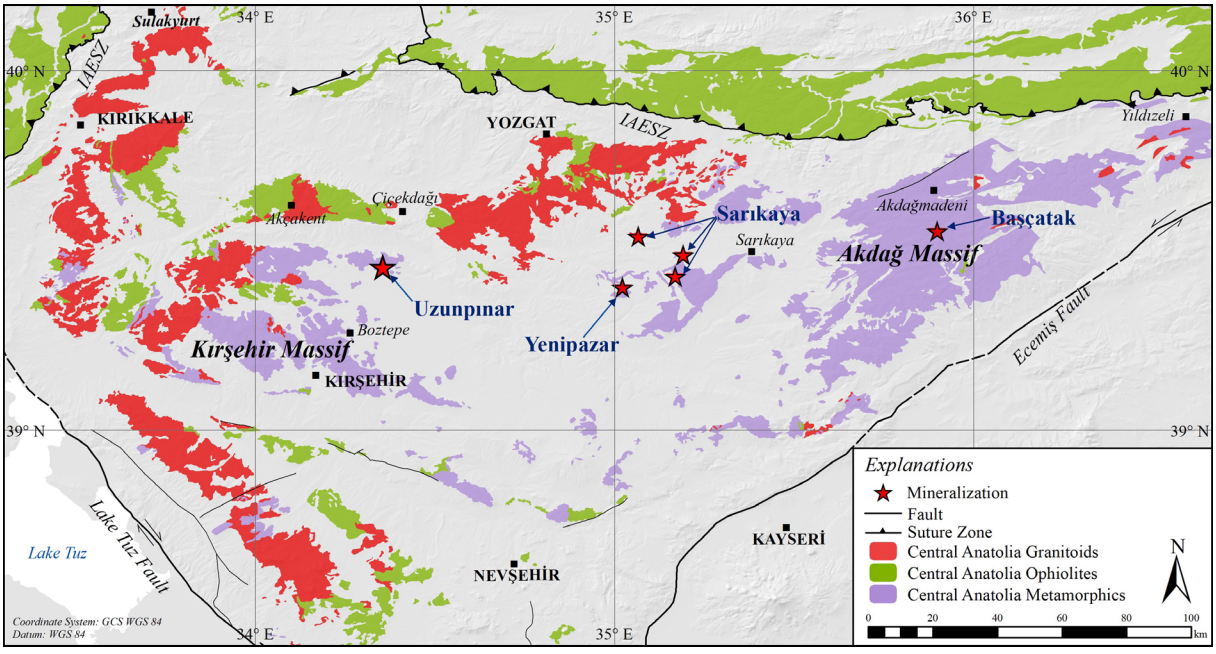

Figure 2- Map showing the location of the Uzunpınar mineralization and major sulfide and iron deposits within the Central Anatolian Crystalline Complex (CACC). The map is compiled from the General Directorate of Mineral Research and Exploration (MTA) 1:500,000-scale geological map (MTA, 2002), with relevant geological units selected. IAESZ: İzmir-Ankara-Erzincan Suture Zone.

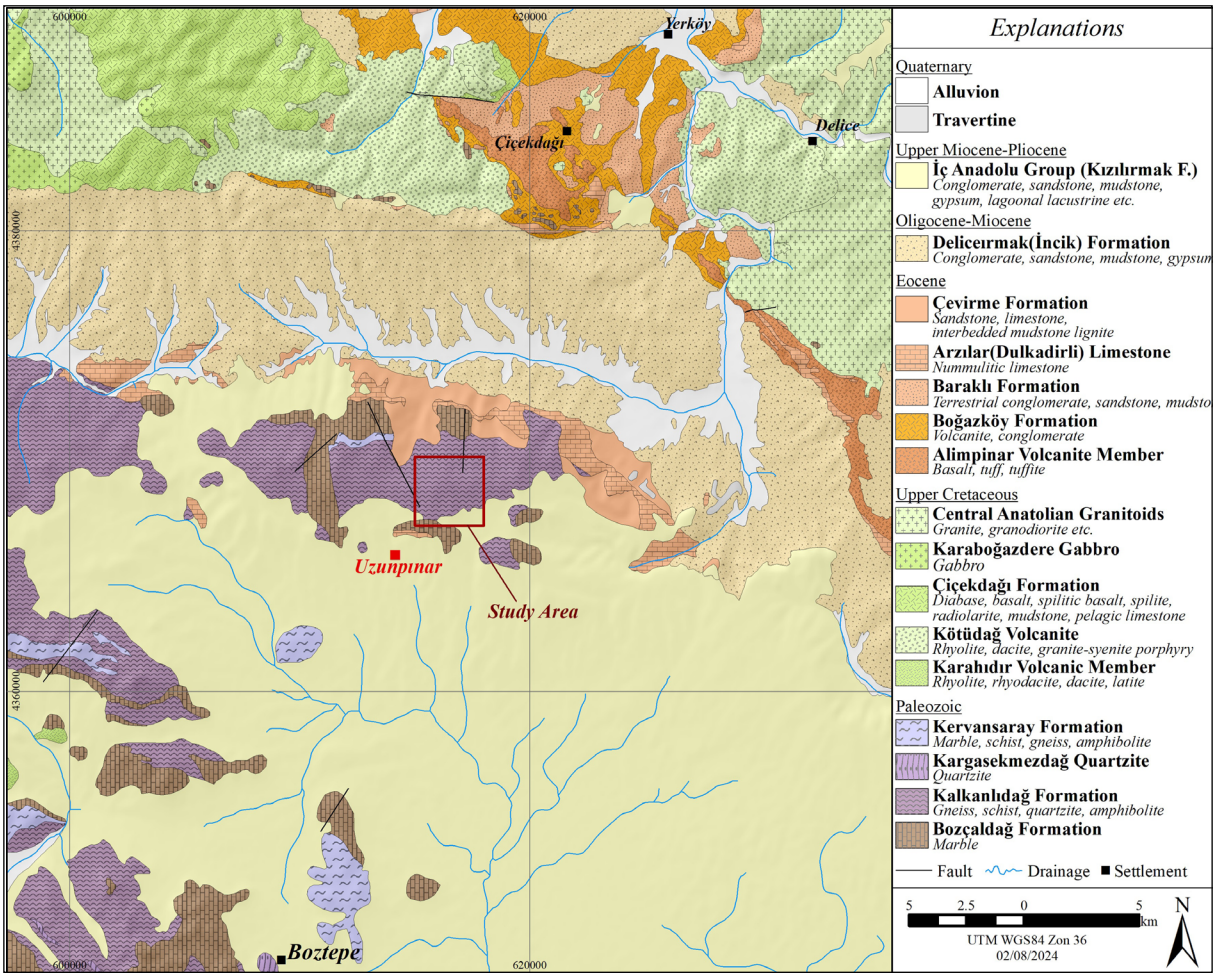

Figure 3- Geological map of the study area. The units shown on the map are compiled from the General Directorate of Mineral Research and Exploration (MTA) 1:100,000-scale sheets İ32 (Dönmez et al., 2005), İ33 (Akçay et al., 2007), J32 (Kara, 1991), and J33 (Kara, 1997).

sequences across the study area. Additionally, microgranite intersected in drill cores represents a distinct unit. Based on metamorphic mineral paragenesis, the metamorphic facies are assigned to the amphibolite and amphibolite-granulite (Erkan, 2006; Bucher and Grapes, 2011). The foliation trends N30E and dips northwest (10–52°). The presence of migmatites and microgranite is interpreted as evidence of partial melting (anatexis) during peak metamorphic conditions.

Gneisses are the most extensively observed unit within the study area and in drill cores. In outcrops, they exhibit gray and light gray colors, whereas drill cores display black, dark gray, gray, and light gray hues. At the hand-specimen scale, foliation is characterized by cm- to dm-scale banding and planar alignment of dark- and light-colored minerals. They are broadly classified as garnet-mica gneiss and sillimanite-mica gneiss, with interlayers of marble and migmatite. The presence of fibrous and idioblastic sillimanite is a critical indicator of high-grade metamorphic conditions (Erkan, 2006). Garnet-mica gneiss and sillimanite-mica gneiss are distinguished by their mineral composition. In the gneiss, lepidogranoblastic and fibrolepidogranoblastic textures are common. The mineral assemblage in gneisses includes quartz, alkali feldspar, plagioclase, biotite, muscovite, garnet, sillimanite, chlorite, epidote, gahnite (Zn-spinel), calcite, zircon, amphibole, sericite, rutile, apatite, and tremolite.

Migmatites are identified in the drill cores and interlayered with gneisses at multiple levels. At the

hand specimen scale, they exhibit gray and light gray (leucocratic) tones, displaying schlieren and diktyonitic textures, with highly folded foliation, as described by Mehnert (1971). In migmatites, the neosomes are more abundant than the paleosomes. The migmatite texture identified in thin sections is fibrolepidogranoblastic. Common minerals in the migmatites include alkali feldspar, quartz, biotite, muscovite, and plagioclase. Accessory minerals, in order of frequency and abundance, are sillimanite, garnet, chlorite, zircon, epidote, and fluorite.

Marble, interlayered with gneisses, has been identified in outcrops and drill cores as white to light gray in color. The rock is mainly calcite, with quartz near ore zones. It has a granoblastic texture with coarse crystals (>500 μm). Away from ore zones, it becomes almost monomineralic, suggesting the protolith was pure limestone without clay or other impurities (Figure 4).

4. Zn-Pb±Cu Mineralization

The Zn-Pb±Cu mineralization in the study area lacks outcrops; its presence is inferred from

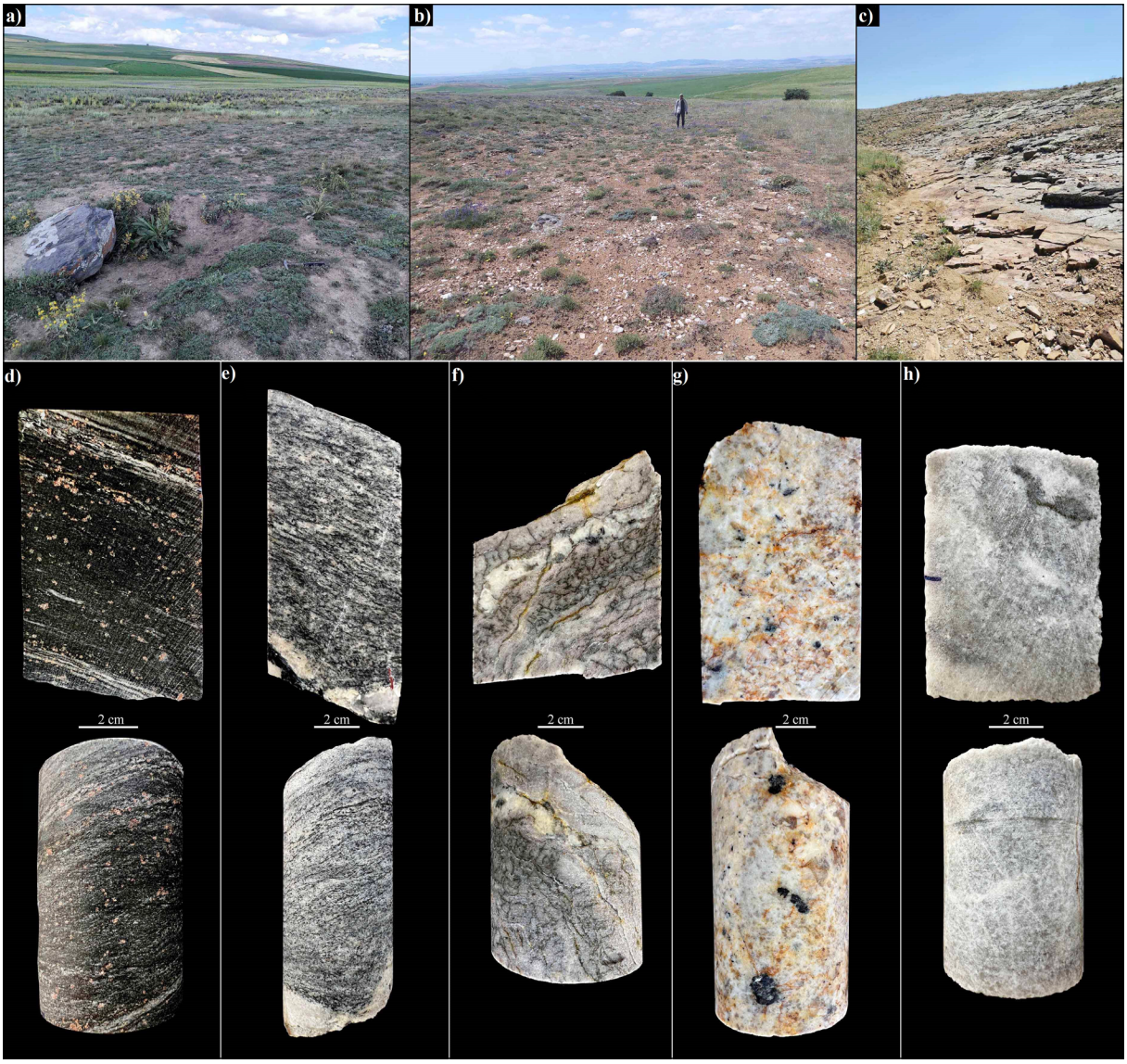

Figure 4- a-c) General views from the study area, d-h) Lithological units observed in outcrops and drill cores, d) Garnet–mica gneiss, e) Sillimanite–mica gneiss, f) Migmatite, g) Microgranite, h) Marble.

weathered-leached floats within the soil cover and from Zn-Pb-Cu anomalies identified in the soil geochemistry survey. The mineralization occurs as foliation-parallel bands and disseminations of variable thickness hosted within marble and gneiss (garnet-mica gneiss and sillimanite-mica gneiss). Integration of drill core data, floats, and geochemical anomalies has delineated six mineralization levels. Four of these levels correlate spatially with floats trends and geochemical soil anomalies. All levels are parallel and extend about 1,850 meters in a northeast-southwest direction. Host rock outcrops follow the same strike and dip northwest.

Based on drill core and surface data, the mineralization levels have been numbered from shallow to deep 1 to 6 according to their stratigraphic position (Figures 5 and 6). Data obtained from drill holes BSK01, BSK05, and BSK06 in the northwest, and BSK02, BSK03, and BSK04 in the southeast confirm the subsurface continuity of the ore-bearing levels in these areas.

The garnet-mica gneisses, which host the mineralization, are typically black to dark gray in color. Medium- to coarse-grained garnet minerals are commonly observed as disseminated grains both

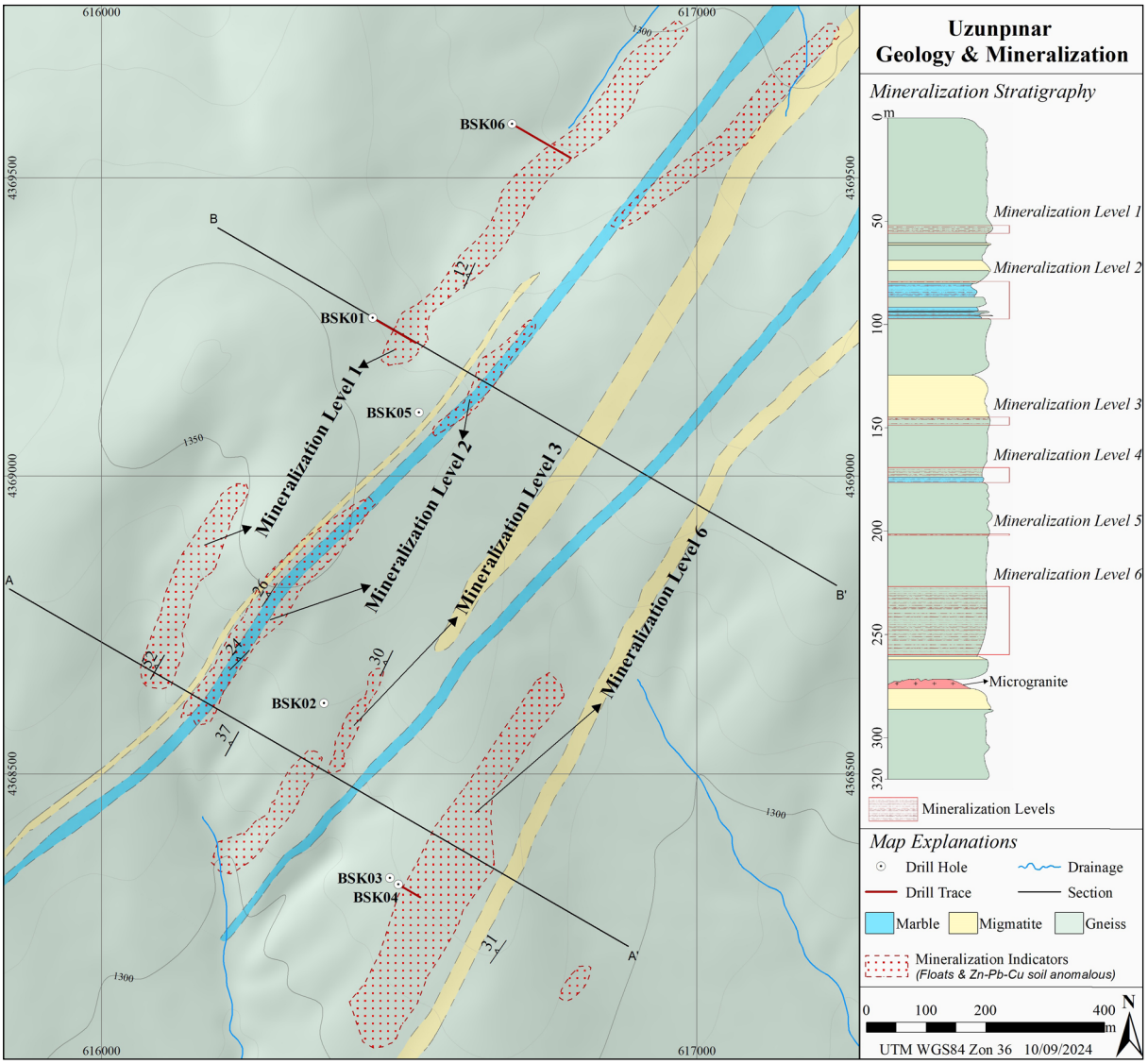

Figure 5- Geology-mineralization map illustrating the ore-bearing levels identified through surface studies and drill data. The stratigraphic section, depicting the mineralization stratigraphy, was constructed by interpreting drill core and surface data. The depth-constrained section is presented without scale on the x-axis.

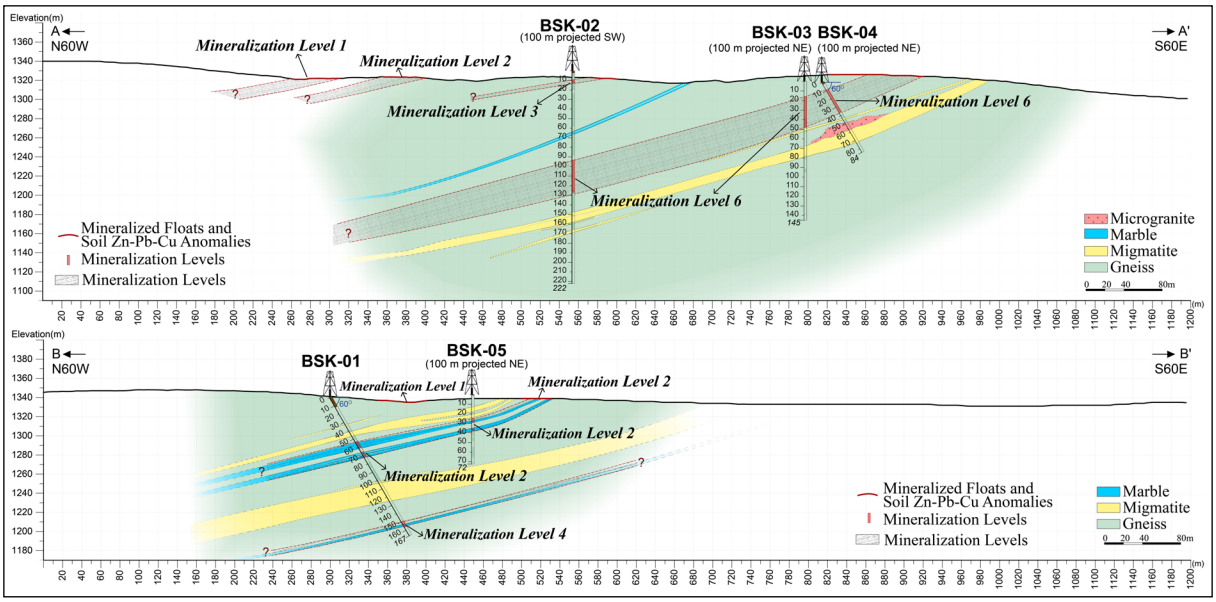

Figure 6- Cross-section AA' and BB' shown on the map in Figure 5. The figure presents correlations between surface mineralization traces and subsurface ore-bearing levels intersected in drill holes.

in the host rock and within the ore-bearing zones. Sphalerite-rich brown ore bands are predominantly hosted by garnet-mica gneisses. In sillimanite-mica gneisses, distinct elongations along foliation planes between disseminated ore minerals and sillimanite crystals have been clearly observed at a microscopic scale. Within the marble units, sphalerite-rich bands appear black to brown, while pyrite-rich bands exhibit a yellow hue. Weathered ore-bearing levels in the marble display yellow, red, and orange colors due to iron oxide minerals and their staining. Cavities formed by the dissolution of weathered and leached sulfide minerals are common in these zones.

Geochemical analyses were conducted on a total of 24 core samples (GS747-GS770) from ore-bearing levels. Nineteen samples were collected from drill hole BSK01, three from BSK06, and two from BSK04. The analytical results for these samples are presented in Table 1. Evaluation of the results reveals that the highest Zn, Pb, and Cu values were detected in samples from the marble-hosted intervals of ore-bearing levels 2 and 4. Geochemical data are not available for Levels 1, 3, 5, and 6; however, the presence of ore in these levels has been confirmed through detailed examination of the core samples and microscopy studies.

The mineralization is characterized by banded textures and coarse- to fine-grained opaque mineral dissemination. The mineralization levels consist of ore minerals in 0.1–8 cm thick bands and disseminations (Figure 7). The number of bands within these levels varies depending on the stratigraphic position and host unit. The total thickness of the levels ranges from 3.1 to 32.10 m. Locally observed, very thin (<1 mm) bands containing ore minerals were not classified as distinct ore-bearing levels. Similarly, zones with pyrite disseminations at low abundances (<1%) were also excluded from ore zone classification. Hand specimen and microscopic studies confirm that ore bands align with the host rock foliation, and alignment of opaque minerals exhibit orientations consistent with the metamorphic texture. Sphalerite is the dominant ore mineral within the bands. Subordinate ore minerals include galena, chalcopyrite and scheelite. Gangue minerals are pyrite, marcasite, pyrrhotite, gahnite, willemite, hematite, limonite, calcite, quartz, barite, Ba-feldspar, apatite, rutile, and ilmenite (Figure 8).

The correlation between surface mineralization traces and mineralization levels intersected in drill holes indicates that the mineralization and foliation planes of the host rocks share the same orientation. These findings support the interpretation that the

Table 1- The analytical results of the core samples are presented thematically. A value of '0' denotes measurements under the detection limit.

Sample ID	Hole ID	Start (m)	End (m)	Sample Length (m)	Au ppm	Ag ppm	As ppm	Cu ppm	Zn ppm	Zn %	Pb ppm	Pb %	Fe %	S %	Mn %	Ba ppm	Mo ppm	Sb ppm	Sn ppm	Sr ppm	Bi ppm	Ni ppm	Co ppm	Cr ppm	Te ppm	Cd ppm	U ppm	Th ppm	Ti %	W ppm	Zr ppm
GS747	BSK01	53.70	54.60	0.90	0.004	0.0	0	**504**	**20100**	**2.01**	**228**	**0.02**	**12.24**	1.72	1.52	**788**	9.4	6	0	53	30	10	40	138	0	**52**	0	0	0.12	0	18
GS748	BSK01	54.60	55.40	0.80	0.000	0.0	3	**220**	**1334**	**0.13**	54	0.01	1.82	0.08	0.30	44	6.0	0	0	153	30	2	7	33	0	4	0	0	0.00	0	22
GS749	BSK01	55.40	56.20	0.80	0.000	0.0	4	10	132	0.01	82	0.01	0.25	0.02	0.16	40	3.1	0	0	160	29	7	5	12	0	0	0	0	0.00	0	18
GS750	BSK01	56.20	57.25	1.05	0.000	0.0	1	20	295	0.03	**334**	**0.03**	0.62	0.03	0.20	41	4.1	0	0	142	28	3	6	42	0	0	0	0	0.00	0	20
GS751	BSK01	57.25	58.30	1.05	0.000	0.0	3	7	125	0.01	55	0.01	0.27	0.07	0.12	20	2.5	0	0	156	28	1	6	17	0	0	0	0	0.00	0	19
GS752	BSK01	58.30	59.30	1.00	0.000	0.0	7	9	61	0.01	38	0.00	0.19	0.05	0.16	25	2.4	0	0	160	31	0	11	17	0	0	0	0	0.00	0	18
GS753	BSK01	59.30	60.30	1.00	0.000	0.0	0	9	71	0.01	76	0.01	0.30	0.15	0.30	22	3.3	0	0	184	26	1	10	13	0	0	0	0	0.00	0	6
GS754	BSK01	60.30	61.30	1.00	0.000	0.0	0	14	475	0.05	**204**	**0.02**	0.76	0.12	0.38	30	5.6	0	0	162	36	3	12	25	0	3	0	0	0.00	0	6
GS755	BSK01	61.30	61.80	0.50	0.000	0.0	2	16	117	0.01	23	0.00	0.60	0.13	0.24	41	3.5	0	0	169	29	12	5	31	0	0	0	0	0.00	0	8
GS756	BSK01	66.60	67.55	0.95	0.000	0.0	11	**158**	**1369**	**0.14**	**364**	**0.04**	2.16	1.69	0.15	228	3.4	0	0	187	30	2	5	18	0	5	0	0	0.00	0	21
GS757	BSK01	68.15	69.35	1.20	0.000	0.0	6	43	**731**	**0.07**	**572**	**0.06**	1.48	0.58	0.19	**346**	**11.1**	0	0	263	30	4	6	20	0	4	0	0	0.00	0	28
GS758	BSK01	70.40	71.55	1.15	0.000	0.0	9	67	**1317**	**0.13**	**680**	**0.07**	1.03	0.90	0.12	**877**	5.5	0	0	185	28	3	7	22	0	6	0	0	0.00	0	14
GS759	BSK01	71.55	72.70	1.15	0.000	0.0	0	25	277	0.03	**106**	**0.01**	1.10	0.66	0.11	**1399**	**10.0**	0	0	273	23	3	7	24	0	1	0	0	0.03	0	26
GS760	BSK01	152.40	153.25	0.85	0.000	0.0	0	**106**	**462**	**0.05**	**185**	**0.02**	5.95	0.46	0.17	**1221**	7.7	0	0	125	0	66	39	224	0	0	0	8	0.59	0	33
GS761	BSK01	153.25	154.00	0.75	0.010	0.0	2	36	**8270**	**0.83**	**3065**	**0.31**	3.07	0.46	0.97	51	2.5	0	0	148	28	8	17	28	0	23	0	0	0.05	0	25
GS762	BSK01	154.00	154.80	0.80	0.019	0.0	3	92	**6030**	**0.60**	**2029**	**0.20**	**6.61**	0.79	0.50	**850**	3.1	0	0	165	0	43	50	163	0	19	0	7	0.76	0	27
GS763	BSK01	154.80	155.55	0.75	**0.176**	2.1	8	**569**	**29500**	**2.95**	**6963**	**0.70**	3.31	2.27	0.26	161	2.7	0	0	317	23	9	21	28	0	**99**	0	0	0.03	0	20
GS764	BSK01	155.55	156.80	1.25	0.004	1.2	2	76	**1991**	**0.20**	**1202**	**0.12**	**6.08**	0.40	0.22	**1154**	4.6	0	0	106	0	48	35	182	0	5	0	5	0.42	0	27
GS765	BSK01	159.20	160.30	1.10	0.085	**4.4**	5	**1457**	**10200**	**1.02**	**2867**	**0.29**	**6.12**	1.57	0.38	**7731**	2.6	0	0	251	0	33	31	456	0	26	0	9	0.34	0	37
GS766	BSK04	50.75	52.75	2.00	**0.121**	**6.1**	**218**	25	**957**	**0.10**	**1017**	**0.10**	1.43	0.14	0.14	388	**9.9**	**21**	0	55	0	12	8	206	0	8	0	0	0.05	0	9
GS767	BSK04	57.10	59.75	2.65	0.014	1.5	15	34	394	0.04	**237**	**0.02**	2.28	1.59	0.05	**15200**	**14.5**	0	0	340	0	23	20	223	0	1	0	7	0.10	0	40
GS768	BSK06	40.85	41.90	1.05	0.000	0.0	2	**109**	274	0.03	95	0.01	3.11	0.67	0.05	**1707**	**29.1**	0	0	111	0	11	16	357	0	0	0	21	0.16	0	63
GS769	BSK06	89.75	90.35	0.60	0.008	0.0	11	12	343	0.03	**393**	**0.04**	1.31	0.26	0.22	**1204**	**10.2**	0	0	51	0	7	10	163	0	0	0	0	0.06	0	23
GS770	BSK06	174.65	175.55	0.90	0.002	0.0	3	48	**2449**	**0.24**	**385**	**0.04**	**6.06**	4.05	0.05	**4810**	**12.7**	0	0	147	0	28	29	279	0	2	0	6	0.22	0	67
Detection Limit					0.001	0.5	1	1	1		2		0.01	0.01	0.002	1	1	5	5	1	5	1	1	1	5	1	5	5	0.01	5	1
Min					0.000	0.0	0	7	61	0.01	23	0.00	0.19	0.02	0.05	20	2.4	0	0	51	0	0	5	12	0	0	0	0	0.00	0	6
Max					0.176	6.1	218	1457	29500	2.95	6963	0.70	12.24	4.05	1.52	15200	29.1	21	0	340	36	66	50	456	0	99	0	21	0.76	0	67
Mean					0.018	0.6	13	153	3636	0.36	886	0.09	2.84	0.79	0.29	1599	7.1	1	0	169	18	14	17	113	0	11	0	3	0.12	0	25

primary geometry of the mineralization may be stratiform. Microscopic observations during thin-polished section studies revealed a consistent alignment and orientation between opaque minerals and rock-forming minerals in the majority of samples. These textures are distinctly observed both in ore bands and in disseminated opaque minerals. These features suggest that the mineralization formed contemporaneously with the protolith of the host rock.

5. Effects of Metamorphism on Mineralization

Distinct effects of high-grade metamorphic processes are observed in the geometry, texture, and mineralogy of the mineralization in the Uzunpınar. The primary indicators of metamorphic effects in the Uzunpınar include: the alignment of ore bands with the foliation planes of the host rocks; co-linear elongation of opaque minerals and metamorphic minerals; the presence of coarse-grained (>100 µm), recrystallized, and euhedral opaque minerals; foam textures (triple-junction) observed in opaque minerals (commonly in pyrites); the presence of gahnite and barium feldspar minerals; the association of pyrite and pyrrhotite; and the high iron content in sphalerites.

In thin sections, alignment and elongation in metamorphic minerals are highly characteristic. Furthermore, opaque minerals observed as disseminations and bands around metamorphic minerals exhibit the same alignment and elongation, which are determined to be parallel to the foliation planes. In sections where sillimanite and mica minerals are common, these alignments and elongations

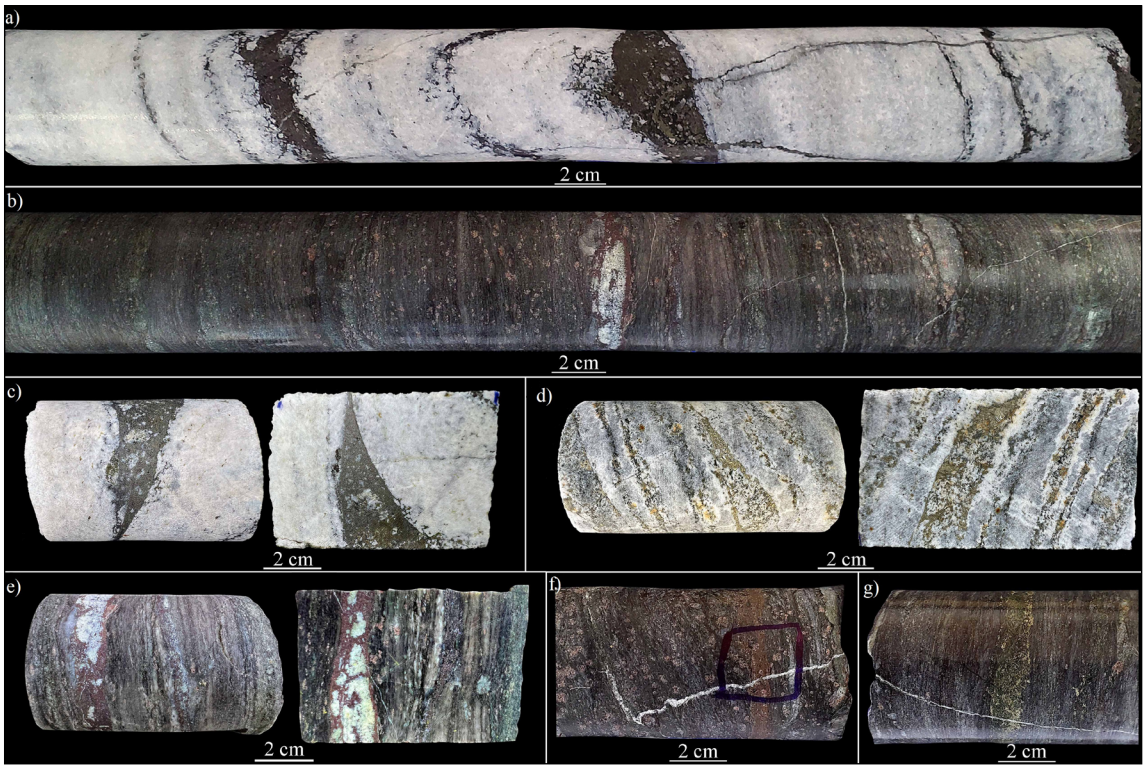

Figure 7- Examples of ore bands identified in drill cores, a) Black-brown sphalerite-rich ore bands within marble, b) Brown sphalerite-rich ore bands within garnet-mica gneiss, c) Sphalerite-rich ore band sample collected from the core shown in image a, d) Yellow pyrite-rich ore bands within marble, e) Sphalerite-rich ore band sample collected from the core shown in image b, f) Brown sphalerite-rich ore band within garnet-mica gneiss, g) Yellow pyrite-rich ore band within garnet-mica gneiss.

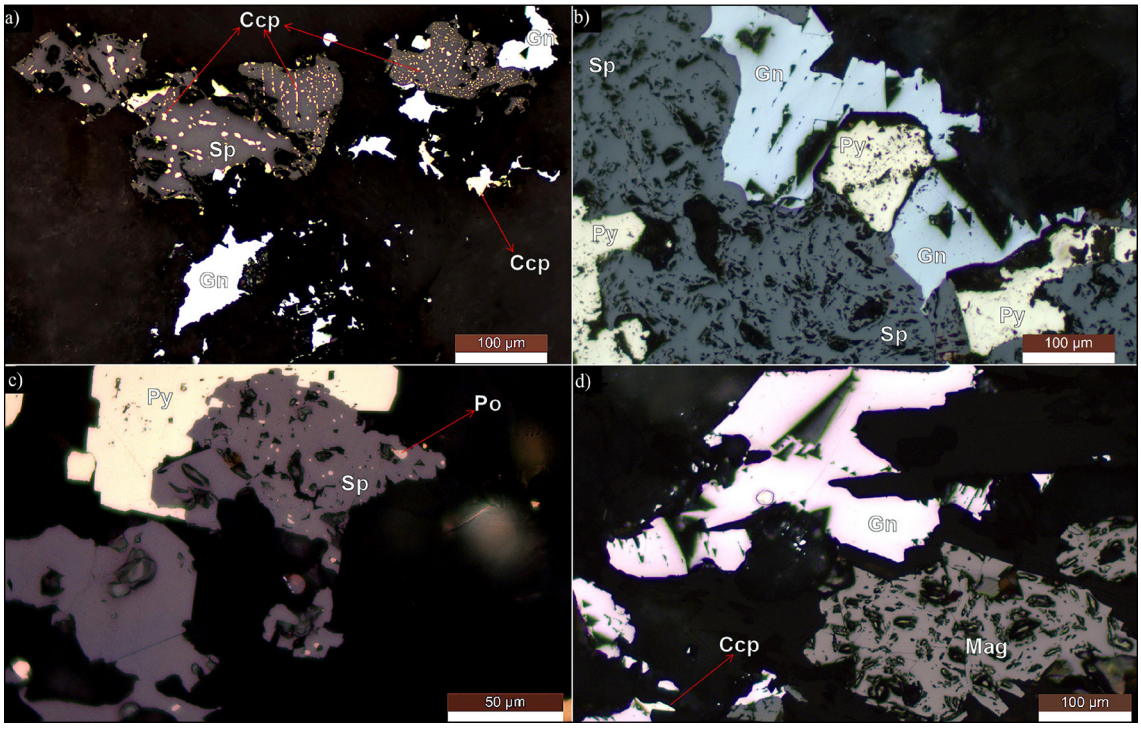

Figure 8- Ore microscopy images of polished section samples obtained from drill cores, a) Sphalerite and galena grains are shown, with chalcopyrite exsolutions within the sphalerite, b) Association of sphalerite, galena, and pyrite, c) Pyrite and sphalerite containing fine pyrrhotite inclusions, d) Galena associated with magnetite and chalcopyrite. Sp: Sphalerite, Gn: Galena, Py: Pyrite, Po: Pyrrhotite, Ccp: Chalcopyrite, Mag: Magnetite.

are more pronounced. Although elongations are predominantly distinct in pyrites, directional textures and elongations caused by metamorphism have also been identified in sphalerites (Figure 9). In stratiform deposits affected by regional metamorphism, one of the prominent deformation effects is the alignment and elongation of ore and ore minerals parallel to the foliation (Vokes, 1998).

In Uzunpınar, particularly observed textural changes include foam textures and euhedral opaque minerals within the samples (Figure 10). Foam textures are observed both among coarse-grained (>100 µm) pyrite minerals and between pairs of opaque minerals (Figure 10 a, b, c). The foam texture (triple junction) is a microstructure that develops due to annealing and recrystallization, minimizing grain boundary surface areas and reducing interfacial tension. In monomineralic ores, interfacial angles approach 120°, whereas in polymineralic ores, these angles vary depending on the minerals present (Craig and Vaughan, 1994). During annealing, smaller grains are absorbed by larger grains (Craig and Vaughan, 1994).

Thin section and polished sample studies reveal significant variation in the grain sizes of opaque minerals. A general assessment indicates that nearly all samples contain coarse-grained (>100 µm) opaque minerals. Euhedral pyrite grains are observed both as individual crystals and in clusters (Figure 10 d). Under metamorphic conditions, recrystallization typically leads to grain size increase (Vokes, 1998). Numerous studies have documented a general rise in pyrite grain size with higher metamorphic grades. In metamorphosed ores with low pyrite content, pyrite often remains confined to mineral interfaces as lenticular masses or triangular aggregates. Conversely, the presence of significant or dominant amounts of other sulfides generally promotes the recrystallization of pyrite into euhedral grains (Craig and Vokes, 1993).

Another significant finding regarding the effects of metamorphism on the Uzunpınar mineralization is the presence of gahnite (Zn-spinel), identified in thin-section and SEM studies. In samples containing gahnite, quartz bands, feldspars, mica minerals, opaque minerals, and garnet are commonly observed around gahnite (Figure 11). Barium feldspar minerals (celsian and hyalophane) detected in SEM studies further indicate metamorphic influences on the mineralization's mineralogy (Figure 11 c, d). The formation of such feldspars is primarily associated with the breakdown of barite and metamorphic processes (Chabu and Boulegue, 1992).

Gahnite ($ZnAl_2O_4$) minerals are commonly observed in exhalative deposits typically subjected to high-grade regional metamorphic conditions. The presence of gahnite is considered a key indicator of deposits having undergone metamorphism (Corriveau and Spry, 2014) and forms under upper amphibolite-

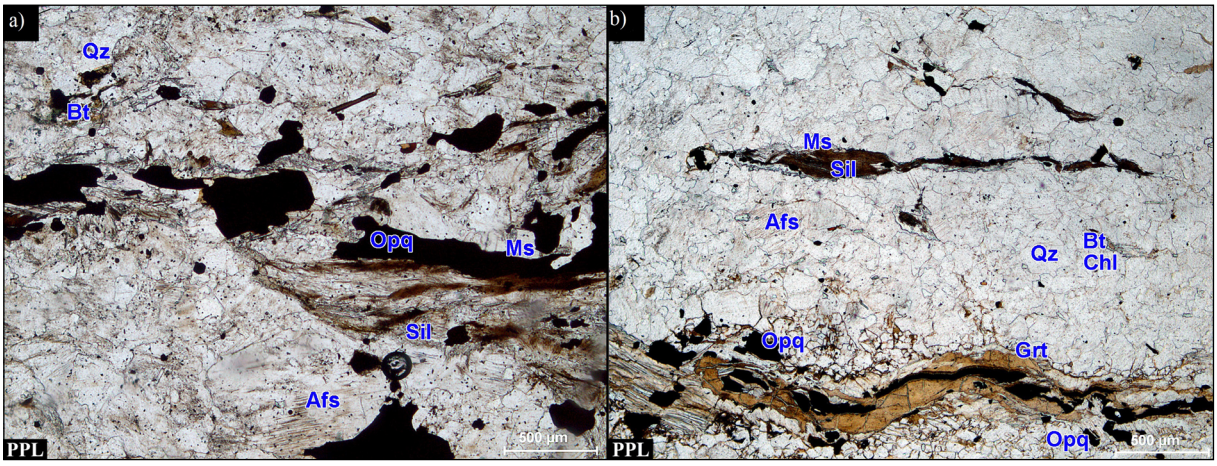

Figure 9- Thin section images showing elongation and alignment in opaque minerals, a) Opaque minerals exhibiting elongation parallel to the orientation of sillimanite, b) Opaque minerals displaying elongation parallel to foliation. PPL: Plane polarized light, Opq: Opaque mineral, Sil: Sillimanite, Grt: Garnet, Afs: Alkali feldspar, Qz: Quartz, Pl: Plagioclase, Bt: Biotite, Ms: Muscovite, Chl: Chlorite.

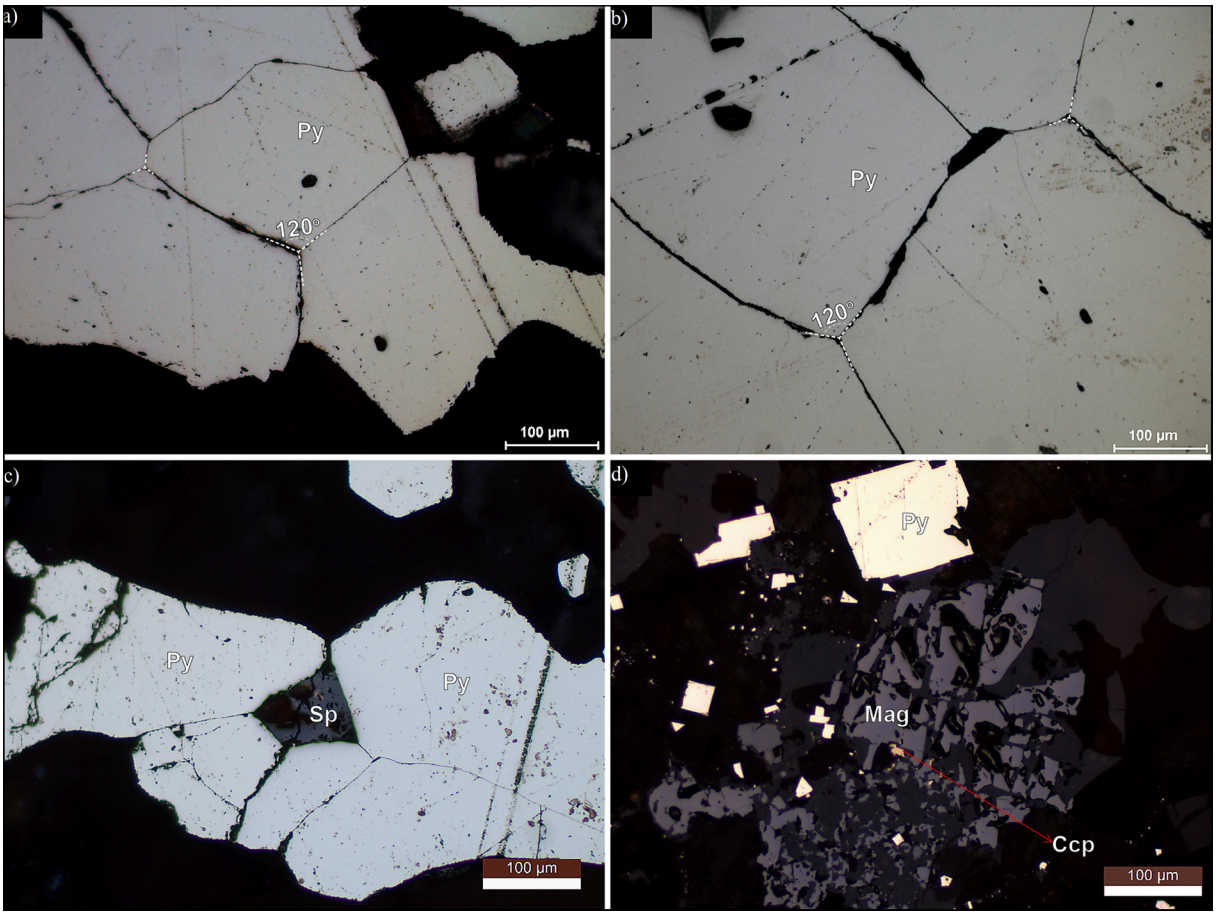

Figure 10- Ore microscopy images of samples exhibiting foam texture and euhedral pyrites, a) and b) Show approximately 120° angles and foam textures observed between coarse-grained (>100 µm) pyrite crystals, c) Sphalerite occurs between pyrite grains, with similar interfacial angles observed between the crystals, d) Displays euhedral pyrite crystals. Py: Pyrite, Sp: Sphalerite, Ccp: Chalcopyrite, Mag: Magnetite.

granulite facies conditions (600–650 °C, 4–5 kbar) (Spry, 1987; Baswani et al., 2022).

The trace amounts of scheelite identified during SEM and ore microscopy studies may also be linked to the effects of metamorphism on the mineralization. Although scheelite is typically associated with magmatic and contact metamorphic processes, evidence suggests it can also form through regional metamorphism (Altenberger et al., 2024). In the Broken Hill Zn-Pb-Ag mineralization (Australia), the presence of scheelite has been reported to correlate with remobilization processes, a known consequence of metamorphism (Plimer, 1994).

In ore microscopy studies, the observed association of pyrite and pyrrhotite in the samples (Figure 12) may be interpreted as an indicator of metamorphic effects in Uzunpınar. At high metamorphic grades, pyrite content decreases due to its breakdown into FeS and S. Conversely, pyrrhotite abundance increases as a result of pyrite decomposition and sulfidation of other Fe-bearing minerals. This trend becomes particularly pronounced near the upper greenschist-amphibolite facies boundary. Some changes induced by prograde metamorphic processes may be reversed during retrograde metamorphism (Marshall et al., 1998).

In sphalerite-rich samples from Uzunpınar, sphalerites frequently exhibit red-brown internal reflection colors (Figure 13a). The intense red and brown internal reflection colors observed in sphalerites indicate high iron content within these minerals (Pracejus, 2008). SEM-EDS analyses of sphalerites confirm Fe contents of ~7% (Figure 13b, c, d), supporting this finding. One of the effects of

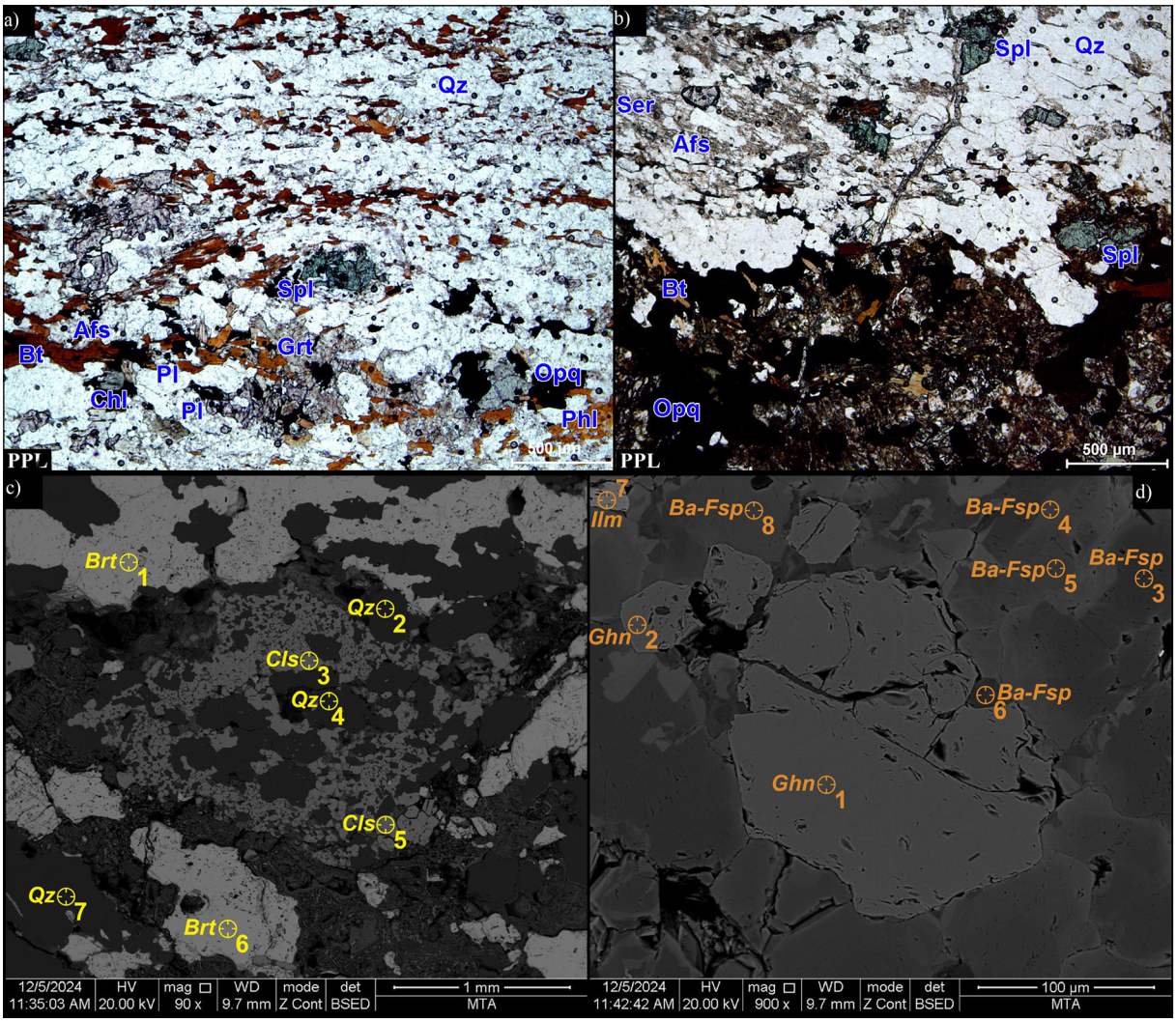

Figure 11- a) and b) Thin section images showing gahnite (Zn-spinel) minerals, c) and d) SEM images are provided. PPL: Plane polarized light, Spl: Gahnite, Grt: Garnet, Opq: Opaque mineral, Afs: Alkali feldspar, Qz: Quartz, Pl: Plagioclase, Bt: Biotite, Phl: Phlogopite, Ser: Sericite, Ghn: Gahnite, Brt: Barite, Cls: Celsian, Ba-Fsp: Barium feldspar-hyalophane, Ilm: Ilmenite.

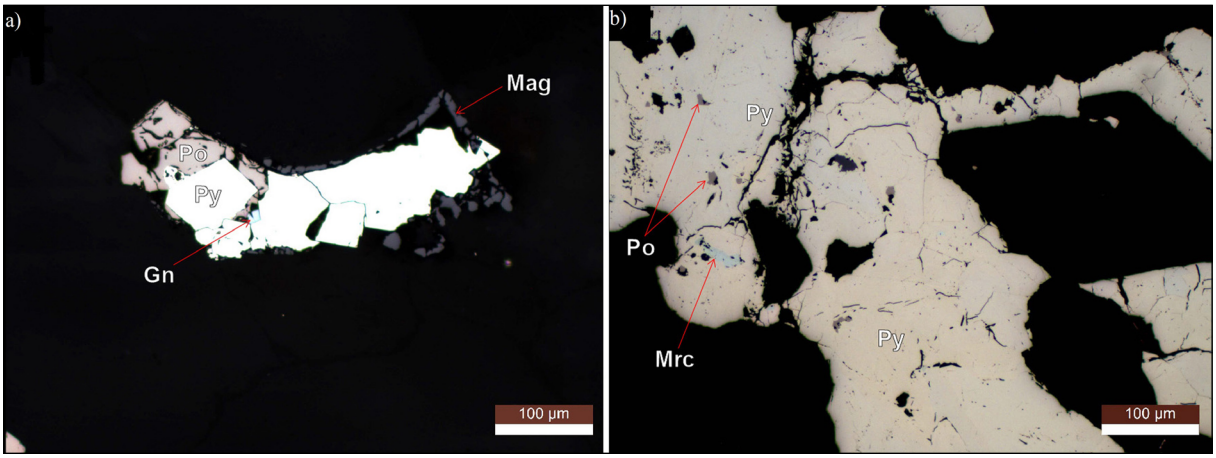

Figure 12- Ore microscopy images. a) Euhedral pyrite crystals, b) Pyrrhotite and marcasite within pyrite. Py: Pyrite, Po: Pyrrhotite, Mrc: Marcasite, Mag: Magnetite, Gn: Galena.

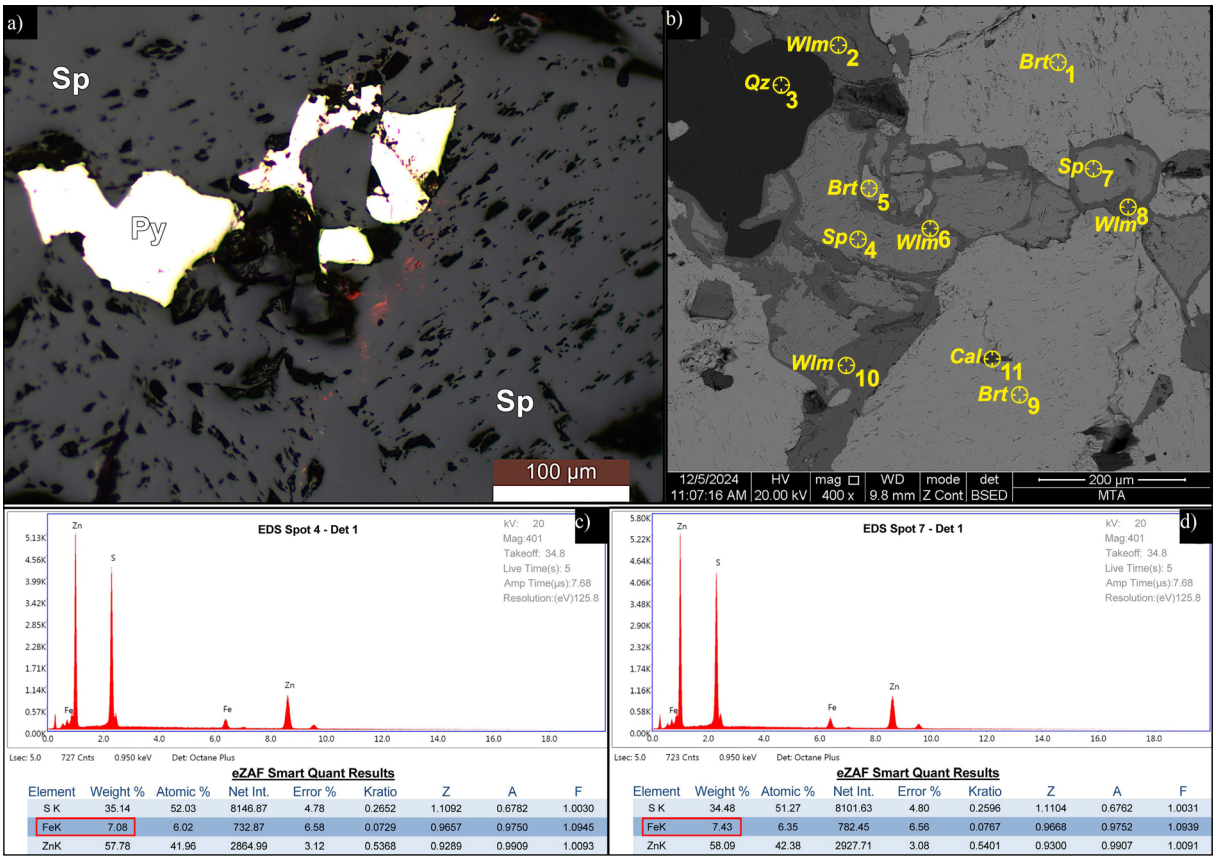

Figure 13- a) Ore microscopy image of sphalerites (plane polarized light); characteristic red internal reflection colors in the minerals are highlighted with red arrows, b) SEM image of sphalerite minerals, c) and d) Present EDS analysis results for these minerals. Sp: Sphalerite, Py: Pyrite, Qz: Quartz, Brt: Barite, Cal: Calcite, Wlm: Willemite.

metamorphism on sphalerites is a gradual increase in FeS percentage with rising metamorphic grades (Bethke and Barton, 1971).

6. Discussion

The geological, mineralogical, and geochemical characteristics of the Uzunpınar Zn-Pb±Cu mineralization point towards a syngenetic origin that has been subsequently overprinted by regional metamorphism. This section discusses these characteristics first within the regional framework of the Central Anatolian Crystalline Complex (CACC) and subsequently places the findings in a broader context by comparing them with global sediment-hosted base metal deposits, notably Sedimentary Exhalative (Sedex) and Broken Hill Type (BHT) deposits.

6.1. Regional Correlation within the CACC

The findings from the Uzunpınar deposit are not isolated within the CACC. When evaluated alongside other known mineralizations in the CACC, a compelling regional metallogenic picture emerges, suggesting a shared paleo-tectonic environment.

The Başçatak Pb-Zn-Cu Deposit: The Başçatak deposit, located within the same metamorphic sequence, shows the most striking similarities to Uzunpınar. Both are hosted by gneisses and marbles, interpreted as metamorphosed pelitic and calcareous sedimentary rocks deposited in a marine environment (Genç, 2001; Coşkun, 2009). Critically, both exhibit a stratiform morphology, with ore bands and disseminations strictly parallel to the host rock's foliation. The mineral assemblages are also analogous, dominated by sphalerite, galena, pyrite, and chalcopyrite, with the presence of pyrrhotite.

Genç (2001) already proposed an exhalative sedimentary origin for Başçatak, an interpretation fully supported by our data for Uzunpınar. The main noted difference is the presence of graphite and organic material at Başçatak, which, while not yet identified at Uzunpınar, is a common feature in many Sedex systems (Emsbo et al., 2016).

The Yenipazar Polymetallic Deposit: The Yenipazar deposit shares several key features with Uzunpınar and Başçatak, including its stratiform nature within a metasedimentary sequence (biotite-schists and marbles) and a mineral assemblage comprising pyrite, chalcopyrite, galena, sphalerite, and gahnite. It has been interpreted as a metamorphosed Volcanogenic Massive Sulfide (VMS) deposit of the Besshi-type (Jacobs Minerals, 2013). The similarities in host rock, morphology, and mineralogy between Yenipazar and the sediment-hosted Uzunpınar/Başçatak deposits highlight the genetic interplay between sedimentary-exhalative and volcanic-exhalative processes in rift-related basins. The presence of cross-cutting breccia zones at Yenipazar may represent a later, feeder-related phase not preserved at Uzunpınar.

The Sarıkaya Fe-Mn Occurrences: Although a different deposit type, the stratiform Sarıkaya Fe-Mn mineralizations, hosted by the same meta-sedimentary package, are significant. Sedimentary iron and manganese formations are known to occur on the peripheries of Sedex basins (Hannington, 2021). The spatial association of Sarıkaya with Uzunpınar, Başçatak, and Yenipazar strengthens the model of a widespread, extensional marine basin where various hydrothermal systems were active.

Synthesis of Regional Context: The collective evidence from these deposits strongly suggests that the CACC hosts a metallogenic province comprising several metamorphosed syngenetic base metal deposits. Their shared characteristics—stratiform morphology, concordance with metamorphic structures, and syngenetic features—indicate a common origin in a rift-related marine basin during the protolith's deposition. The variations in metal content (Zn-Pb vs. Cu-Au-Ag vs. Fe-Mn) can be attributed to differences in the specific hydrothermal vent systems and their position within the paleo-basin.

6.2. Global Context: A Comparison with Sedex and BHT Deposit Models

To further constrain the genetic model for Uzunpınar, its characteristics are compared below with two classes of stratiform base metal deposits: Sedex and BHT.

6.2.1. Comparison with Sedex Deposits

The Uzunpınar mineralization displays numerous characteristics aligning it with the Sedex deposit model:

Host Rock and Depositional Environment: The protoliths of the host garnet-mica gneisses (shales, siltstones) and marbles (limestones) are typical of the fine-grained, marine sedimentary sequences that host Sedex deposits (Leach et al., 2005; Emsbo et al., 2016). The interpreted marine depositional environment for the Kalkanlıdağ Formation (Seymen, 1981, 1984) is consistent with a Sedex-forming rift basin.

Ore Morphology and Texture: The key evidence is the stratiform nature of the mineralization, defined by thin, laterally continuous ore bands parallel to the lithological layering and foliation. This is a hallmark of Sedex deposits, which form as layered sulfide accumulations on the seafloor (Hannington, 2021). The observed banded and disseminated textures are primary sedimentary textures preserved despite metamorphism.

Mineralogy and Metal Content: The primary ore mineral assemblage of sphalerite + galena + pyrite ± chalcopyrite is classic for Sedex deposits. The presence of barite and apatite at Uzunpınar is also a common feature in many Phanerozoic and Proterozoic Sedex systems, respectively (Leach et al., 2005).

A significant feature of many Sedex deposits is the presence of a sub-seafloor "feeder zone". The lack of an obvious feeder conduit at Uzunpınar does not preclude a Sedex model. It is well-established that high-grade metamorphism can obliterate or transpose such discordant features into sulfide-rich schists, making them indistinguishable from the stratiform ore (Vokes, 1998). Furthermore, the "distal" subtype of Sedex deposits, which accounts for over 80% of

known occurrences, often lacks well-defined feeder zones at the deposit scale (Leach et al., 2005). Uzunpınar can thus be robustly interpreted as a metamorphosed distal Sedex-type deposit.

6.2.2. Comparison with Broken Hill Type (BHT) Deposits

Given the high-grade metamorphic overprint, a comparison with the high-grade BHT deposits is also warranted.

Similarities: Both Uzunpınar and BHT deposits are hosted by high-grade metasedimentary rocks (granulite to amphibolite facies) and exhibit strong structural control. The Zn-Pb-dominated metal suite and the stratiform, lens-like morphology are shared characteristics. The presence of minerals like gahnite (Zn-spinel) at Uzunpınar is highly significant, as these are considered characteristic gangue mineral in BHT environments (Spry and Teale, 2021).

Differences: Key distinctions from classic BHT deposits include the generally much larger size and higher Ag grades of the latter (e.g., Broken Hill, Cannington) (Spry and Teale, 2021). Furthermore, BHT deposits are characterized by a distinct accessory element suite (e.g., Sb, Bi, Au) and are associated with specific rock types like quartz-garnet rocks (coticules) and iron formations, which are not reported at Uzunpınar (Leach et al., 2005). The amount of pyrrhotite at Uzunpınar also appears lower than in typical BHT deposits. A fundamental difference lies in the mineralization age; whereas most major BHT deposits are Paleoproterozoic to Mesoproterozoic (e.g., the ~1.7 Ga Broken Hill deposit), the Uzunpınar mineralization is hosted by lithologies of the Central Anatolian Crystalline Complex, which are significantly younger (Walters and Bailey, 1998).

The origin of BHT deposits is controversial, with models ranging from highly metamorphosed Sedex deposits to a unique class (Sangster, 2020). The strong similarities of Uzunpınar with Sedex deposits in terms of protolith environment and primary mineralogy suggest that its fundamental genesis is Sedex-related. The BHT-like characteristics, such as gahnite, can be explained as a result of the high-grade metamorphic reconstitution of a pre-existing Sedex protore. Therefore, Uzunpınar can be best described as a metamorphosed Sedex deposit that exhibits some features transitional to the BHT spectrum.

7. Results

The Zn-Pb±Cu mineralization is hosted by gneisses (garnet-mica gneiss, sillimanite-mica gneiss) and marbles. The mineralization exhibits a stratiform geometry, concordant with the foliation of the host rocks. The mineralization comprises six distinct mineralization levels (horizons), dominated by sphalerite, galena, pyrite, and chalcopyrite, occurring as ore bands and disseminations. The thickness of the ore bands ranges from 0.1 to 8 cm, while the mineralization levels vary in thickness between 3.1 and 32.10 m. The ore bands align with the host rock foliation, and disseminated opaque minerals also display a parallel orientation to the host rock minerals. Opaque minerals occur as both coarse-grained (>100 μm) and fine-grained (<50 μm) phases. The primary ore mineral is sphalerite. Subordinate ore minerals within the bands include galena, chalcopyrite, and trace amounts of scheelite. Gangue minerals consist of pyrite, marcasite, pyrrhotite, hematite, limonite, gahnite, willemite, calcite, quartz, barite, barium feldspar (celsian and hyalophane), apatite, rutile, and ilmenite. Pyrrhotite, gahnite, barium feldspar, and scheelite are interpreted to have formed due to metamorphic effects.

The Uzunpınar mineralization has been demonstrated to represent a metamorphosed sulfide mineralization, as evidenced by the findings. Morphological, textural, and mineralogical changes observed in the mineralization reflect the effects of high-grade regional metamorphism. Key indicators of metamorphic influence on the mineralization include: the concordance of ore bands with the foliation planes of the host rocks; the presence of coarse-grained (>100 μm) and euhedral opaque minerals; foam textures; the occurrence of gahnite and barium feldspar; the association of pyrite and pyrrhotite; high iron content in sphalerites; and co-linear elongation of opaque and metamorphic minerals.

The Uzunpınar (Zn-Pb±Cu), Başçatak (Pb-Zn-Cu), Yenipazar (Cu-Pb-Zn-Au-Ag), and Sarıkaya (Fe-Mn) mineralizations are situated along an east-west-trending belt within the Kırşehir and Akdağ massifs and are interpreted to have formed under similar genetic conditions. The syngenetic character of these deposits, their sedimentary-derived protoliths, and their stratiform structure suggest that the ores developed in regionally analogous geological settings.

The morphological, mineralogical, and geological features of the Uzunpınar mineralization strongly indicate its classification as a sedimentary exhalative (SEDEX) deposit. The stratiform geometry of the mineralization is evident from foliation-parallel, banded structures within the mineralization levels. The protoliths of the host rocks (gneisses and marbles), comprising pelitic-carbonate sediments with intercalated carbonate layers, indicate a marine depositional environment. Index minerals such as mica, sillimanite, and garnet further confirm the high-grade metamorphism of these pelitic protoliths. The occurrence of gahnite, barium feldspars, scheelite, and quartz-rich bands within the mineralization levels represents hydrothermal exhalites enriched in Zn, Ba, and Si. These findings collectively support the interpretation that the Uzunpınar mineralization represents a syngenetic SEDEX-type deposit that was originally formed by the exhalative discharge of metal-rich hydrothermal fluids onto a marine seafloor and later underwent high-grade metamorphism.

Acknowledgement

This research was conducted as part of the first author's master's thesis at Hacettepe University. The author expresses gratitude to the university for providing the necessary support and facilities during the study.

References

Akçay, A. E., Dönmez, M., Kara, H., Yergök, A. F., Esentürk, K. 2007. MTA, 1/100,000 ölçekli Türkiye Jeoloji Haritaları No:80 Yozgat - İ33 paftası. Maden Tetkik ve Arama Genel Müdürlüğü, Ankara.

Altenberger, F., Krause, J., Wintzer, N. E., Iglseder, C., Berndt, J., Bachmann, K., Raith, J. G. 2024. Polyphase stratabound scheelite-ferberite mineralization at Mallnock, Eastern Alps, Austria. Mineralium Deposita 59(1), 1109–1132.

Bakanyıldız, M. 1973. Sarıkaya Metamorfik Demir Madeninin Jeolojisi. Rapor No: 4951, Maden Etüt ve Arama Dairesi Başkanlığı, Ankara (unpublished).

Baswani, S. R., Mishra, B. P., Mahapatro, S. N., Meshram, T., Pati, P., Shareef, M., Korakoppa, M., Mishra, M., Raza, M. A., Roy, S., Randive, K., Malviya, V. P., Dora, M. L. 2022. Petrochemical evaluation of gahnite from volcanogenic massive sulfide deposits in Betul belt, Central India: Insight from petrography and in-situ trace element geochemistry. Geological Journal 57(11), 4508-4528.

Bethke, P. M., Barton, P. B. 1971. Distribution of some minor elements between coexisting sulfide minerals. Economic Geology 66, 140–156.

Bucher, K., Grapes, R. 2011. Metamorphic grade. In: Bucher, K., Grapes, R. (Eds.). Petrogenesis of Metamorphic Rocks. Springer, Berlin, Heidelberg, 85–120.

Chabu, M., Boulegue, J. 1992. Barian feldspar and muscovite from the Kipushi Zn-Pb-Cu deposit, Shaba, Zaire. Canadian Mineralogist 30, 1143–1152.

Corriveau, L., Spry, P. G. 2014. Metamorphosed hydrothermal ore deposits. Geological Survey of Canada, Natural Resources Canada, Quebec, Canada. Published by Elsevier Ltd., 175–194.

Coşkun, E. 2009. Akdağmadeni (Yozgat) Pb-Zn Yataklarında Metamorfizma Etkisinin Araştırılması. Doktora Tezi, Hacettepe Üniversitesi Fen Bilimleri Enstitüsü, Ankara.

Craig, J. R., Vaughan, D. J. 1994. Ore Microscopy and Ore Petrography, 2nd ed. Wiley Interscience Publication, Wiley, 120–163.

Craig, J. R., Vokes, F. M. 1993. The metamorphism of pyrite and pyritic ores: An overview. Mineralogical Magazine 57, 3–18.

Çağatay, A., Arda, O. 1976. Yozgat-Sarıkaya Manganezli Demir Yatağının Mineralojik Etüdü. Bulletin of the Mineral Research and Exploration 86, 1-12.

Çolakoğlu, A. R., Genç, Y. 2001. Akdağmadeni (Yozgat) Kurşun-Çinko Yatağının Makro-Mikro Dokusal Özellikleri ve Kökensel Yorumu. Türkiye Jeoloji Bülteni 44(1), 1–12.

Dönmez, M., Bilgin, Z. R., Akçay, A. E., Kara, H., Yergök, A. F., Esentürk, K. 2005. 1/100,000 ölçekli Türkiye

Jeoloji Haritaları No:47 Kırşehir - İ32 Paftası, Maden Tetkik ve Arama Genel Müdürlüğü, Ankara.

Emsbo, P., Seal, R. R., Breit, G. N., Diehl, S. F., Shah, A. K. 2016. Sedimentary exhalative (sedex) zinc-lead-silver deposit model: U.S. Geological Survey Scientific Investigations Report 2010-5070-N, 57.

Erkan, Y. 1978. Kırşehir Masifinde Granat Minerallerin Kimyasal Bileşimi ile Rejyonal Metamorfizma Arasındaki İlişkiler. T.J.K Bülteni 21, 43-50.

Erkan, Y. 1981. Orta Anadolu Masifinin Metamorfizması Üzerine Yapılmış Çalışmalarda Varılan Sonuçlar. T.J.K. 35, Bilimsel ve Teknik Kurultayı İç Anadolu'nun Jeolojisi Sempozyumu, 9-11.

Erkan, Y. 2006. Magmatik Petrografi. Jeoloji Mühendisleri Odası Yayınları Yayın No. 93, Ankara.

Esri, 2017. World Street Map. https://www.arcgis.com/home/item.html?id=de26a3cf4cc9451298ea173c4b324736 (Erişim Tarihi: 26.07.2024).

Genç, Y. 1998. Başçatak-Akdağmadeni (Yozgat) Zn-Pb-Cu Sülfid Yatağı: Akdağmadeni Masifi'nde Metamorfik Sülfid Yatağına Bir Örnek. Üçüncü Uluslararası Türk Jeoloji Sempozyumu, Ankara.

Genç, Y. 2001. Başçatak (Akdağmadeni-Yozgat) Zn-Pb-Cu Sülfid Yatağında Gözlenen Metamorfik Yapı ve Dokular. 54. Türkiye Jeoloji Kurultayı, Bildiri No: 54-51, 7-10 Mayıs, Ankara.

Gökce, A., Canbaz, O., Ünal Çakır, E., Bozkaya, G., Bektaş, Ö., Başdelioğlu, O. 2024. Mineralization characteristics of Lead-Zinc-Copper deposits in Akdağmadeni Region (Northern Central Anatolia, Türkiye): Integration of field study, geochemical, isotope, and geophysical data. Geochemistry 84(4), 126201.

Göncüoğlu, M. C. Toprak, V. Kusçu, İ. Erler, A. Olgun, E. 1991. Orta Anadolu Masifinin Batı Bölümünün Jeolojisi, Bölüm:1, Güney Kesim. TPAO, Rapor No: 2909, 140 (unpublished).

Hannington, M. 2021. VMS and SEDEX deposits. In: Alderton, D., Elias, S. A. (Eds.), Encyclopedia of Geology (Second Edition). Academic Press, 874-887.

Jacobs Minerals Canada Inc. 2013. NI 43-101 Technical Report on the Feasibility Study of the Yenipazar Project, Turkey. Prepared for Aldridge Minerals Inc. Available at: http://s1.q4cdn.com/788688556/files/1879%20NI%2043-101%20MAY%2016,%202013.pdf. Accessed 14 December 2024.

Kara, H. 1991. 1/100.000 Ölçekli Açınsama Nitelikli Türkiye Jeoloji Haritaları No:37 Kırşehir - J32(G18) Paftası, Maden Tetkik ve Arama Genel Müdürlüğü, Ankara.

Kara, H. 1997. 1/100,000 Ölçekli Açınsama Nitelikli Türkiye Jeoloji Haritaları No:54 Yozgat - J33(G19) Paftası, Maden Tetkik ve Arama Genel Müdürlüğü, Ankara.

Ketin, İ. 1955. Yozgat Bölgesi'nin Jeolojisi ve Orta Anadolu Masifinin Tektonik Durumu. Türkiye Jeoloji Bülteni 6, 1-40.

Leach, D. L., Sangster, D. F., Kelley, K. D., Large, R. R., Garven, G., Allen, C. R., Gutzmer, J., Walters, S. 2005. Sediment-hosted lead-zinc deposits: A global perspective. Economic Geology 100th Anniversary, 561-607.

Marshall, B., Vokes, F. M., Larocque, A. C. L. 1998. Regional metamorphic remobilization: Upgrading and formation of ore deposits. Reviews in Economic Geology, Metamorphosed and Metamorphogenic Ore Deposits 11, 19-35.

Mehnert, K. R. 1971. Migmatites and the origin of granitic rocks. Elsevier Publishing Company, Amsterdam, 7-42.

Maden Tetkik ve Arama Genel Müdürlüğü, 2002. 1/500,000 ölçekli Türkiye Jeoloji Haritası.

OpenStreetMap Contributors. 2024. OSM. https://www.openstreetmap.org (Accessed: 26 July 2024).

Plimer, I. R. 1994. Strata-Bound Scheelite in Meta-Evaporites, Broken Hill, Australia. Economic Geology and the Bulletin of the Society of Economic Geologists 89(3), 423-428.

Pracejus, B. 2008. The Ore Minerals Under the Microscope: An Optical Guide. Atlases in Geo-sciences 3, Elsevier, Amsterdam, 178-180.

Sangster, D. F. 2020. Evidence that Broken Hill-type Pb-Zn deposits are metamorphosed SEDEX deposits. Mineralium Deposita 55(7), 1263-1270.

Seymen, İ. 1981. Kaman (Kırşehir) Dolayında Kırşehir Masifinin Stratigrafisi ve Metamorfizması. TJK Bülteni 24, 7-14.

Seymen, İ. 1984. Kırşehir Masifi Metamorfitlerinin Jeolojisi ve Evrimi. TJK Yayını, Ketin Sempozyumu.

Spry, P. G. 1987. The chemistry and origin of zincian spinel associated with the Aggeneys Cu–Pb–Zn–Ag deposits, Namaqualand, South Africa. Mineralium Deposita 22, 262–268.

Spry, P. G., Teale, G. S. 2021. A classification of Broken Hill-type deposits: A critical review. Ore Geology Reviews 139, 103935.

Vokes, F. M. 1998. Ores and metamorphism: Introduction and historical perspectives. Reviews in Economic Geology, Metamorphosed and Metamorphogenic Ore Deposits 11, 1–13.

Walters, S., Bailey, A. 1998. Geology and mineralization of the Cannington Ag-Pb-Zn deposit: an example of Broken Hill-type mineralization in the Eastern succession, Mount Isa Inlier, Australia. Economic Geology 93(8), 1307-1329.

Whitney, D. L., Teyssier, C., Dilek, Y., Fayon, A. K. 2001. Metamorphism of the Central Anatolian Crystalline Complex, Turkey: Influence of orogeny normal collision vs. wrench-dominated tectonics on P-T-t paths. Journal of Metamorphic Geology 19, 411–432.